Extension of Power Transmission Capacity in MMC-based HVDC Systems through Dynamic Temperature-Dependent Current Limits

Jorge Gonçalves, Daniel J. Rogers, Jun Liang
Cardiff University - School of Engineering
Trevithick Building 14-17 The Parade, CF24 3AA
Cardiff, United Kingdom
E-Mail: {GoncalvesJ, RogersDJ, LiangJ1}@cardiff.ac.uk

Acknowledgements

The research leading to these results has received funding from the People Programme (Marie Curie Actions) of the European Union's Seventh Framework Programme FP7/2007-2013/ under REA grant agreement no. 317221, project title MEDOW

Keywords

«Modular Multilevel Converters», «Converter Control», «Power Transmission», «Thermal Stress»

Abstract

This paper proposes the extension of the current control loops used in Modular Multilevel Converters to include semiconductors junction temperature as an operational constraint. A new controller is added to the inner current loop to modulate the current limits as a function of the temperature, providing an extension of the power transmission capacity without violating the thermal limits of the semiconductors. A numerical method to investigate the operation of converters with temperature-dependent current limits is proposed and the stability of the controller is analyzed and validated through simulations under steady and transient operations.

Introduction

The Modular Multilevel Converter (MMC) is a recent VSC-type topology particularly suited for HVDC applications [1] and its general structure is depicted in Figure 1. The Sub-Module (SM) configuration adopted in this work is the Half-Bridge SM (HBSM), composed of two IGBTs and a capacitor. For industrial applications, each arm is composed of hundreds of SMs, with thousands of IGBTs switching to generate a quasi-sinusoidal voltage waveform on the AC side [2].

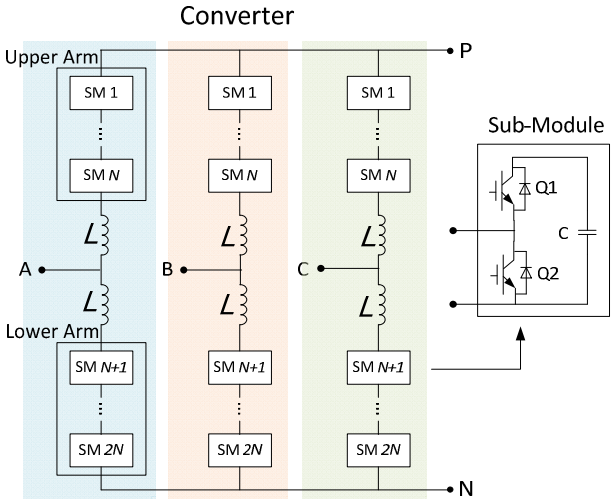

Figure 1 – Structure of the Half-Bridge Modular Multilevel Converter.

Unlike other power system components such as large synchronous generators, lines or transformers, IGBTs possess a very short thermal time constant and therefore have a very limited overload capability. To avoid IGBT over-temperature stresses a current limit is normally implemented in the converter control system [3], [4]. The use of such conventional fixed limits can be viewed as a conservative choice in that it sets the maximum power contribution from the converter, without the possibility to temporarily provide an overload capability. This limitation is particularly relevant when VSC-based multi-terminal DC grids are expected to provide frequency support to a distressed AC grid, by transferring power from a remote energy storage resource or another AC grid [2].

In order to extend the power transmission capability but keep the temperature within safe limits, an active control mechanism must be implemented. In this paper an additional control loop is proposed to set the current limit dynamically in response to the measured semiconductor temperature. The proposed control scheme acts to enforce a current magnitude limit that ensures the electrical and thermal limits are kept within safe bounds. This offers the potential to extend the power transmission capability of the converter when semiconductor junction temperature is below the maximum limit, i.e. there is thermal headroom available.

Modular Multilevel Converter Control

The control of the MMC can be divided into two components [2]: the general "VSC Control" and the particular "MMC Control", represented in Fig. 2 (a). The general control is common to VSC-type topologies and is typically implemented on Park's Reference Frame (*dq0* frame), as depicted in Fig. 2 (b), where the Outer Controllers receive the set points of the high-level control quantities, e.g. Active and Reactive Power Injections and AC and DC voltage magnitudes. These loops provide the *d*- and *q*-components of current (I_d^{ref} and I_q^{ref}, respectively) to the Inner Current Loop which, through a series of cascaded PI controllers, produces a reference voltage $\left(V_{abc}^{ref}\right)$ that the converter should output at its terminals. This reference is sent to the MMC control, where it is used for operations particularly related with the MMC control such as Circulating Current Suppression, Modulation and sub-module (SM) Capacitor Voltage Balancing.

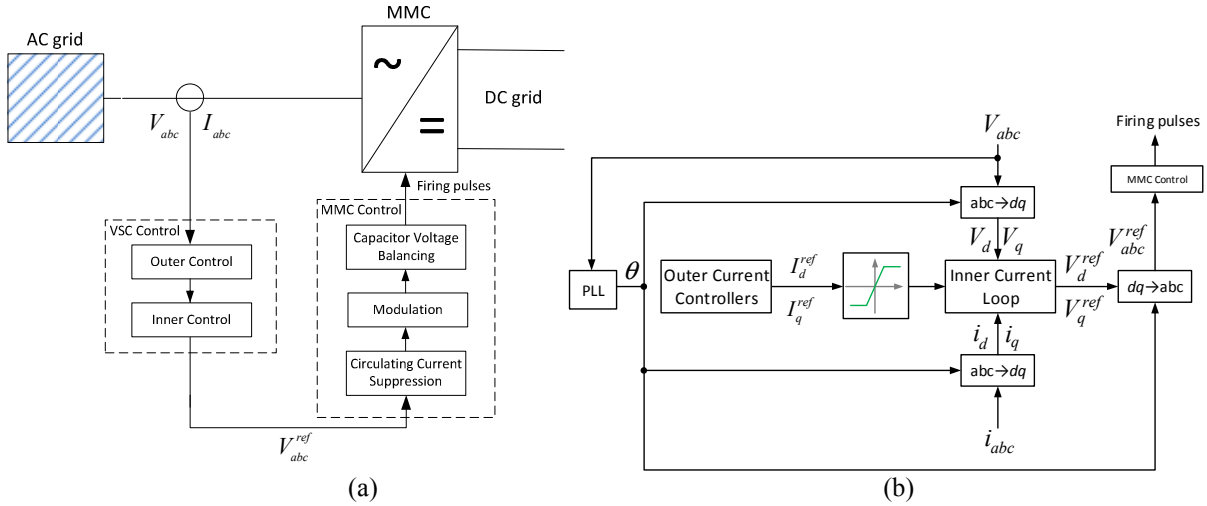

Figure 2 - Modular Multilevel Converter Control: (a) - Structure and (b) - Inner and Outer Current Loops.

In order to ensure that the current through the components in the converter stations stay within their limits, the current reference components are subjected to limits between the outer and inner current loops, as represented in Fig. 2 (b). These limits are set low enough such that the maximum junction temperature of the semiconductor die in the IGBT modules is never violated, even under worst-case operating conditions (e.g. high system voltage and high ambient temperature), however, during other operating conditions (e.g. nominal system voltage and low ambient temperature), the limits prevent the full capability of the converter from being used to support the AC or DC grid.

Active Thermal Control

Electro-Thermal Dynamics

The relationship between the collector current and the operating temperature of an IGBT is defined in its datasheet. For silicon devices, the maximum temperature is normally in the range 125 – 150 °C and this temperature limit must be respected under all conditions to avoid the destruction of the device. Normally the temperature is kept below 100 °C to minimize semiconductor thermal cycling and fatigue effects [5], [6].

The conduction and switching actions of IGBTs generate heat that must be dissipated. This heat is conducted from the heat source, the silicon chip, to the surrounding ambient and this path is composed of layers of different components with different thermal resistances R_{th} and capacitances C_{th}. Losses depend on the physical parameters of the devices, specified in their datasheet, and on their operating conditions (collector-emitter voltage and collector current), therefore electrical and thermal models need to be combined in order to calculate device temperature for any given electrical condition. In this work, the combined electro-thermal model provides an estimation of the temperature in every time step, based on the collector-emitter voltage and collector current of each IGBT module, and on the thermal network that characterizes the heat flow inside each semiconductor module, according to the data sheet information. This process is represented in Fig. 3.

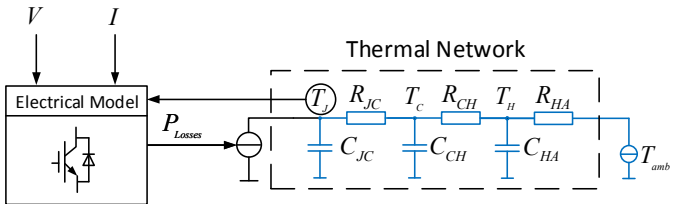

Figure 3 – Electro-Thermal Model for the estimation of the junction temperature.

Proposed Controller

Previous work on the active thermal control of VSCs modules has focused essentially on the control of the switching frequency [7]–[9] as a means to reduce the temperature of the semiconductors. However this approach is unsuited for MMC applications as they operate at a very low switching frequency [10], in the order of a few hundred Hertz, with little room for further reduction. This low switching frequency is one of the advantages over previous 2- and 3-Level VSC topologies that operate in the range of kilohertz.

In an MMC the temperature rise is almost entirely due to conduction losses as the low switching frequencies make switching losses small [11]. Conduction losses are a function of the current through the IGBTs and diodes in the SMs [11], therefore the control of the junction temperature can only be effectively performed by varying the current magnitude in the SMs, which is, at any moment, common to all the SMs conducting. In this work an additional control loop is proposed to enable the converter control to be sensitive to the junction temperature and ensure that temperature limits are respected at all times by limiting the electrical transmission capability if necessary, i.e. the thermal and electrical limits are defined together and not separately. The proposed control scheme dynamically sets the current limits by following the time behaviour of the temperature. The current limit I_{lim} is defined as:

$$I_{lim}(T_J) = I_{nom} + k \cdot (T_{J(nom)} - T_J) \quad (1)$$

Where T_J is the semiconductor junction temperature estimation, I_{nom} the nominal current limit, i.e. the design current of the system, $T_{J(nom)}$ is the nominal (threshold) operating temperature of the IGBT and is chosen to take into account the long term reliability of the semiconductor and k, defined in

[A/°C], is the temperature-current droop constant, used to define the decrease in the current limit per unit increase in junction temperature. k is defined so that $I_{lim}\left(T_{J(\max)}\right) = 0$, i.e.

$$k = \frac{I_{nom}}{T_{J(max)} - T_{J(nom)}} \tag{2}$$

Where $T_{J(max)}$ is the maximum allowed temperature of the IGBT. Considering the IGBT Module 5SNA 0650J450300 from ABB [12], $T_{J(nom)}$ =80 °C at I_{nom} =550 A and $T_{J(max)}$ = 125 °C. In this case k=12.22 A/°C.

The control law represented by (1) is implemented as represented in Figure 4 (a). Furthermore, the current limit I_{lim} given by (1) corresponds to the absolute current limit through the semiconductors in the converter SMs, i.e.

$$I_{lim} = \sqrt{I_{d\,\mathrm{lim}}^{ref^2} + I_{q\,\mathrm{lim}}^{ref^2}} \tag{3}$$

Where $I_{d\,\mathrm{lim}}^{ref}$ and $I_{q\,\mathrm{lim}}^{ref}$ are the active and reactive current reference limits, respectively. Moreover, (3) only defines the absolute current limit, as the individual components I_d^{ref} and I_q^{ref} are defined by a high-level control according to the application.

When the current limit is modulated, individual d- and q- component limits are proportionally modulated according to the initially set values. This process is illustrated in Figure 4 (b), where an increase in the temperature from T_J^A to T_J^B causes the absolute limit to decrease from I^{ref} to $I^{ref(lim)}$, proportionally modulating the d- and q- current components accordingly:

$$\begin{cases} I_d^{ref(\mathrm{lim})} = \epsilon I_d^{ref} \\ I_q^{ref(\mathrm{lim})} = \epsilon I_q^{ref} \end{cases} \tag{4}$$

Where

$$\epsilon = \frac{I_{lim}(T_J)}{\sqrt{I_d^{ref^2} + I_q^{ref^2}}} \tag{5}$$

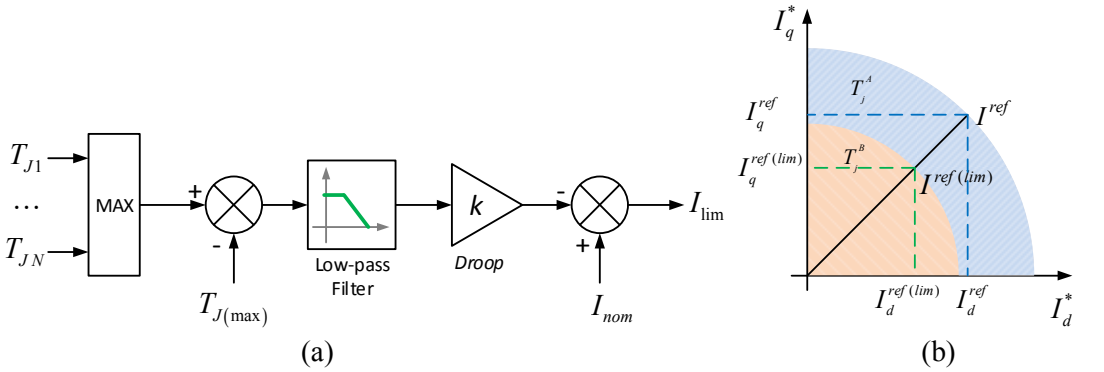

(a) (b)

Figure 4 – Proposed Control Scheme for the current limit: (a) - Dynamic Temperature-Dependent Current Limit Modulator and (b) – Extended Current Limit Diagram with flexible limits for the current references $\left(T_J^A < T_J^B\right)$.

Globally, the proposed control structure of the MMC, with the current limits being dynamically set as a function of the junction temperature, is represented in Figure 5. The other control blocks, for

example, those used to provide circulating current suppression and capacitor voltage balancing for the MMC, are unaltered.

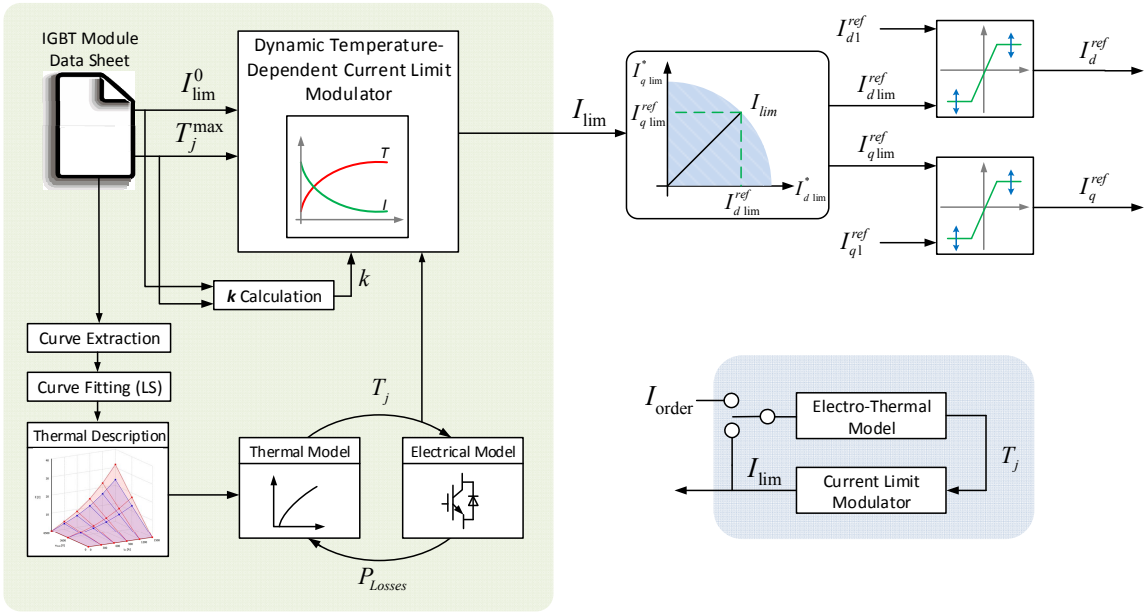

Figure 5 – Simulation model for the MMC with: Dynamic Temperature-Dependent Current Limits (left shaded area) and simplified block diagram of the electro-thermal model for the evaluation of the proposed controller stability (bottom right shaded area).

Although this control could be implemented in 2- and 3-Level, VSC topologies, it is particularly suited for MMCs where conduction loss dominates, directly acting on the current limit to control semiconductors temperature.

Stability of the Controller

When the control is active, the current order will be subjected to the limits imposed by the modulator and defined by the droop equation, as represented in the shaded bottom right area of Figure 5. However, the calculation of the estimation of junction temperature is a function of the thermal network of the IGBT module and the current magnitude.

The thermal network from the IGBT module junction until the ambient temperature is represented in Fig. 3 and T_J, T_C, T_H and T_{Amb} are the estimated Junction, Case, Heat Sink and Ambient temperatures andR_{th} and C_{th} are the thermal resistances and capacitances, respectively. The subscripts refer to which point of the thermal network the resistances and capacitances are connected. Considering the heat flow from one thermal section to the other and the energy balance, the following equations apply:

$$\dot{T}_J = \frac{P_{Losses}}{C_{JC}} - \frac{T_J}{C_{JC}\cdot R_{JC}} + \frac{T_C}{C_{JC}\cdot R_{JC}} \tag{6}$$

$$\dot{T}_C = -\frac{T_C}{C_{CH}}\cdot\left(\frac{1}{R_{JC}} + \frac{1}{R_{CH}}\right) + \frac{T_J}{C_{CH}\cdot R_{JC}} + \frac{T_H}{C_{CH}\cdot R_{CH}} \tag{7}$$

$$\dot{T}_H = -\frac{T_H}{C_{HA}}\cdot\left(\frac{1}{R_{CH}} + \frac{1}{R_{HA}}\right) + \frac{T_C}{C_{HA}\cdot R_{CH}} + \frac{T_{Amb}}{C_{HA}\cdot R_{HA}} \tag{8}$$

Junction temperature T_J is defined as the output value, T_J, T_C and T_H as the state variables and P_{Losses} and T_{Amb} as the inputs. Conduction losses P_{Losses} are essentially driven by the current magnitude and can be described using a 2nd order degree polynomial expression [11]:

$$P_{Losses}(I) = \sigma \cdot I + \rho \cdot I^2 \tag{9}$$

Where the coefficients σ and ρ are derived using a least-squares curve fitting method applied to IGBT datasheet information. Since the current limit is dependent on the temperature in a linear manner given by (1), the losses value is a direct non-linear function of the junction temperature estimation provided by the thermal network, closing the loop.

As shown in Fig. 4 (a), in order to diminish the influence of short-term variations in the junction temperature on the current limit, a low-pass filter was included to smooth the temperature measurement. This low-pass filter also approximates the placement of a temperature sensor a short distance away from the silicon die internal to the IGBT module. A filter cutoff frequency of 10 Hz was used to remove the temperature fluctuations due to IGBT switching actions but leave the longer-term temperature rises intact. This creates another state variable T_F, corresponding to the filtered value of T_J. Using a first order low pass filter with a time constant τ gives:

$$\dot{T_F} = \frac{1}{\tau}\left(T_J - T_F\right) \tag{10}$$

From (1) and (9), one can write:

$$P_{Losses}(T_F) = \alpha + \beta \cdot T_F + \gamma \cdot {T_F}^2 \tag{11}$$

$$\begin{cases} \alpha = \sigma \cdot I_{nom} + \sigma \cdot k \cdot T_{J(nom)} + \rho \cdot I_{nom}^2 + 2 \cdot \rho \cdot k \cdot I_{nom} \cdot T_{J(nom)} + \rho \cdot k^2 \cdot T_{J(nom)}^2 \\ \beta = -2 \cdot \rho \cdot k \cdot I_{nom} - 2 \cdot \rho \cdot k^2 \cdot T_{J(nom)} - \sigma \cdot k \\ \gamma = \rho \cdot k^2 \end{cases} \tag{12}$$

Conduction losses are now a direct (non-linear) function of the state variable T_F. Linearizing (10) around $T_{J(nom)}$ and substituting into (6) allows the writing of a set of differential equations whose time response can be evaluated through the solving of the equations with respect to the state variables T_J, T_C, T_H and T_F. Eqs. (6) - (8) can be rewritten in the canonical state-space form as:

$$\begin{bmatrix} \dot{T}_J \\ \dot{T}_C \\ \dot{T}_H \\ \dot{T}_F \end{bmatrix} = \mathbf{A} \cdot \begin{bmatrix} T_J \\ T_C \\ T_H \\ T_F \end{bmatrix} + \mathbf{B} \cdot \begin{bmatrix} \alpha - \gamma \cdot T_{J(nom)}^2 \\ T_{Amb} \end{bmatrix} \quad \mathbf{T_J} = \begin{bmatrix} 1 & 0 & 0 & 0 \end{bmatrix} \cdot \begin{bmatrix} T_J \\ T_C \\ T_H \\ T_F \end{bmatrix} \tag{11}$$

$$\mathbf{A} = \begin{bmatrix} -\frac{1}{C_{JC} \cdot R_{JC}} & \frac{1}{C_{JC} \cdot R_{JC}} & 0 & \frac{\beta + 2\gamma \cdot T_{J(nom)}}{C_{JC}} \\ \frac{1}{C_{CH} \cdot R_{JC}} & -\frac{1}{C_{th}^{CH}}\left(\frac{1}{R_{JC}} + \frac{1}{R_{CH}}\right) & \frac{1}{C_{CH} \cdot R_{CH}} & 0 \\ 0 & \frac{1}{C_{HA} \cdot R_{CH}} & -\frac{1}{C_{HA}}\left(\frac{1}{R_{CH}} + \frac{1}{R_{HA}}\right) & 0 \\ \frac{1}{\tau} & 0 & 0 & -\frac{1}{\tau} \end{bmatrix} \quad \mathbf{B} = \begin{bmatrix} \frac{1}{C_{JC}} & 0 \\ 0 & 0 \\ 0 & \frac{1}{C_{HA} \cdot R_{HA}} \\ 0 & 0 \end{bmatrix} \tag{12}$$

The analysis of the stability can be evaluated through the analysis of the eigenvalues of the **A** matrix. The controller will be stable if all the eigenvalues have negative real parts. From (1) it can be seen that the tunable parameter of the control law is the gain k, appearing implicitly in the **A** matrix through β and γ, and it is the control parameter dictating the stability of the system. The thermal network parameters were considered from the IGBT Module 5SNA 0650J450300 from ABB [12] and the current limit modulator was parameterized according to the data sheet parameters, as represented in Table I.

Table I: DTCL Controller and Thermal Network Parameters

Control Parameters		Curve Fitting		Section	R_{th} (°C/W)	C_{th} (J/°C)
I_{lim}^{0} (A)	650	b (W/A)	1.711	CH	3.95	6
$T_{J(nom)}$ (°C)	85	c (W/A^2)	0.002901	HA	5.2	30
$T_{J(max)}$ (°C)	125					

The eigenvalues of the linearized system were determined for different values of the gain k in the range 10-30 A/°C and the temperature was varied over a wide expected operating range, including extreme values, 0-150 °C, for the controller defined by (2). Results are represented in Fig. 6 (a) and (b), respectively, where the lines represent the critical damping ratio $\zeta = 1$.

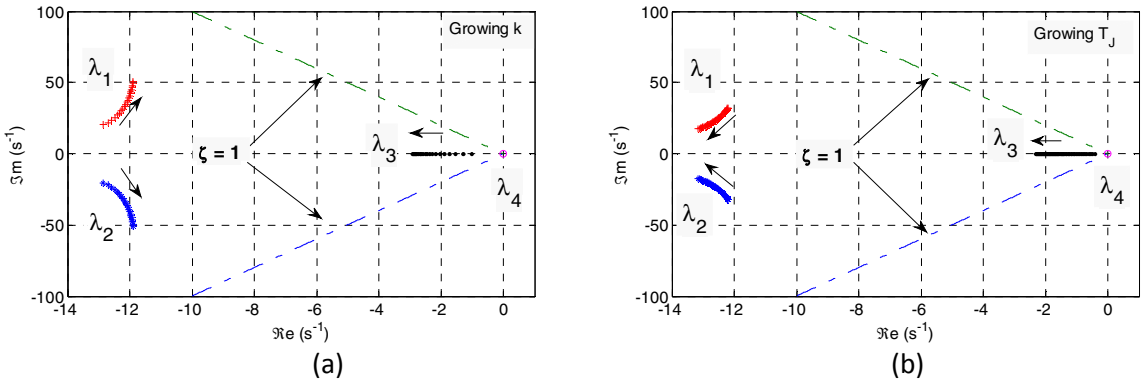

Figure 6 – Eigenvalues of the system: (a) - As a function of the controller gain k and (b) – As a function of the temperature.

The system has four eigenvalues, in the form of two real poles and a complex conjugate pair. It remains stable across the k and T_J ranges given above and is characterized by a dominant real pole close to the real axis (time constant of 67.9-69.3 s). The damping ratios very between 2.28 and 5.35 for the k range and 3.55 and 6.03 for the T_J range. Since the complex poles have a damping ratio greater than a critical value, they are overdamped and the temperature will never overshoot.

Simulation Results

The controller was evaluated through two case studies: response to an overload request and operation under fault conditions. The converter is operating as an inverter and the junction temperature is calculated for all the sub-modules and the maximum value in each moment is used by the dynamic temperature-dependent Current Limit Modulator block, as represented in Fig. 4 (a). Since only the electro-thermal dynamics is of interest, a reduced number of SMs (10) was used in the detailed model implemented in MATLAB/Simulink using the PLECS toolbox [13], in order to keep the simulation time acceptable. The data of the case study is represented in Table II.

Table II: Case Study Data

AC System Data		MMC and DC System Data	
V_{AC} (kV)	15	V_{DC} (kV)	±15
P (MW)	9.0 (1.0 p.u.)	#SM	10
P_{limit} (p.u.)	± 1.1	V_{cap} (kV)	3.0
L_{AC} (mH)	5	C_{SM} (mF)	5
f (Hz)	50	L_{Arm} (mH)	3
		f_c (Hz)	500

Response to an overload request

The converter maintains a unity power factor and the initial set-point sent to the control level is P = 9 MW (1.0 p.u.). At t = 6.0 s the power order is changed to 1.15 p.u, (P = 10.35 MW) to simulate the request of extra power, for instance to balance the power deficit in the AC Grid, requiring the converter to operate in an overload mode. The dynamic current limit controller is activated at t = 8.0 s and the response of the semiconductors temperature, current limit and transmitted power are illustrated in Fig. 7 (a), (b) and (c), respectively.

The junction temperatures reach a thermal steady state in approximately 5.0 s, as represented in Fig. 7 (a), where the initial temperature increase was omitted. When the new power order is issued, the converter is initially capable of providing the requested power, shown in Fig. 7 (c), disregarding the fixed limit, as shown in Fig. 7 (b). The junction temperature starts to increase, reaching the threshold value around 7.5 s. When the current limit controller is activated at t = 8.0 s, it detects that the temperature is above the threshold value and decreases the current limit, restricting the maximum transmitted power to 10.13 MW (1.13 p.u.). Since the current now is below the threshold value, the temperature is allowed to be slightly higher than 80 °C and stabilizes. When the power order is set to the initial value of 1 p.u. at t = 13.0 s, the temperature starts to decrease and the controller correspondingly increases the current limit.

With the proposed controller the converter is capable of providing additional power for 5 s. The converter could operate at 1.13 p.u. permanently since this operating point satisfies both electrical and thermal restrictions. However, this feature is especially valuable in emergency conditions, as the overload time is sufficient to aid the primary frequency response of the generators connected to the AC grid, helping the post-contingency frequency recovery.

Response to a fault

Figure 8 represents the performance of the controller under a 100 ms AC Phase-to-Ground Fault at 6 s. The high fault current magnitude causes an increase in the temperature which in turn leads to a decrease in the current order and the injected power. After the fault is cleared and the temperature starts to decrease, the current limit increases accordingly. Therefore, the controller is able to deliver additional Fault Ride-Through response by taking into account the temperature of the semiconductors and exploiting the additional thermal headroom available. It can also be seen that there is a small delay between the temperature increase and the decrease of the current limit in this case. This is a consequence of the low-pass filter included in the current limit modulator, and can be seen with detail in Fig. 8 (c).

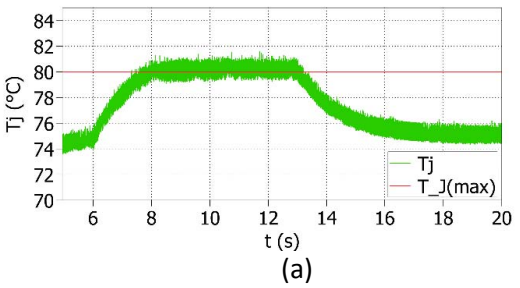

(a)

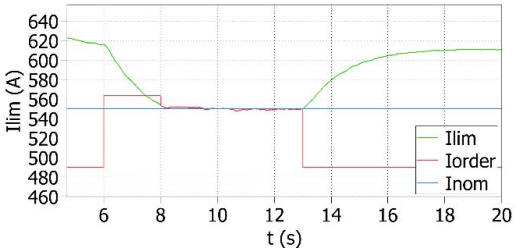

(b)

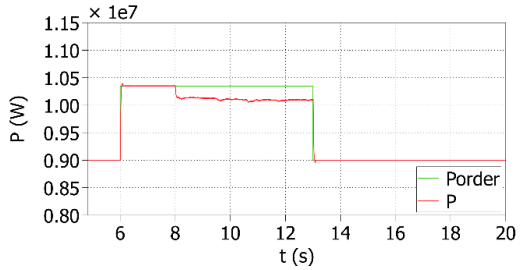

(c)

Figure 7 – Response of the MMC under a power order change with dynamic current limits: (a) – Estimated junction temperature; (b) – Current Limit Modulation and (c) – Requested and Injected Active Power.

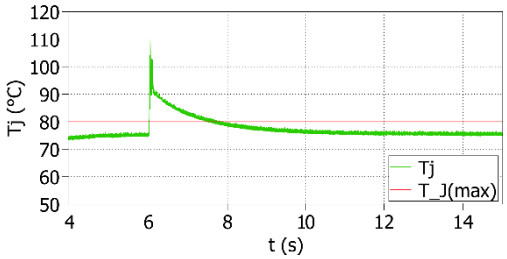

(a)

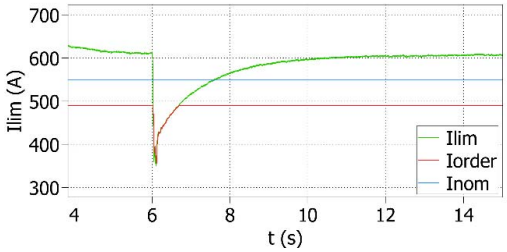

(b)

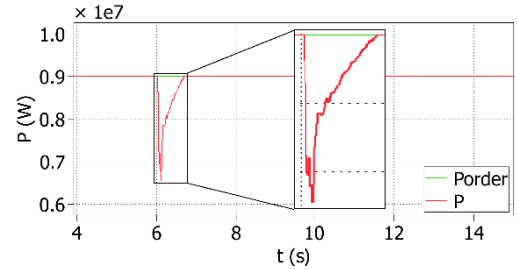

(c)

Figure 8 – Response of the MMC under an AC Phase-to-Ground fault with dynamic current limits: (a) – Estimated junction temperature dynamics; (b) – Current Limit Modulation and (c) – Requested and Injected Active Power.

Conclusion

This work proposes a controller that maximizes the output capabilities of a VSC converter by ensuring the full utilization of the thermal headroom of the semiconductor devices. The controller is particularly suited for MMC-based HVDC systems and through the implementation of dynamic current limits allows the converter to provide additional power transmission capability while ensuring that semiconductor temperature is kept within safe boundaries at all times.

A theoretical analysis and a methodology to analyze the operation of a MMC with dynamic temperature-dependent current limits was proposed, as well as a method for choosing the control gain k. The dynamic equations of the system were represented in a state-space form and the stability of the system for a range of k and T_J was evaluated. Simulation results show that the proposed method works as intended and ensures that the junction temperature stays below the maximum value.

The previous analysis assumed ideal temperature measurements, albeit with a lag associated with the low pass filter. Making such measurements would not necessarily be possible in a practical semiconductor module. Measurements in the real world will be limited by sensor placement, noise and additional delays and filtering that will affect the dynamics of system and could potentially lead to poor or unstable behavior. The next step of this work will be to validate the control system design presented here in laboratory hardware.

References

[1] A. Lesnicar and R. Marquardt, “An innovative modular multilevel converter topology suitable for a wide power range,” in *Power Tech Conference Proceedings, 2003 IEEE Bologna*, 2003, vol. 3, p. 6 pp. Vol.3.

[2] H. Saad, J. Peralta, S. Dennetiere, J. Mahseredjian, J. Jatskevich, J. A. Martinez, A. Davoudi, M. Saeedifard, V. Sood, X. Wang, J. Cano, and A. Mehrizi-Sani, “Dynamic Averaged and Simplified Models for MMC-Based HVDC Transmission Systems,” *Power Deliv. IEEE Trans.*, vol. 28, no. 3, pp. 1723–1730, 2013.

[3] C. Q. Du, M. H. J. Bollen, E. Agneholm, and A. Sannino, “A new control strategy of a VSC-HVDC system for high-quality supply of industrial plants,” *Ieee Trans. Power Deliv.*, vol. 22, no. 4, pp. 2386–2394, 2007.

[4] Y. Liu and Z. Chen, “A Flexible Power Control Method of VSC-HVDC Link for the Enhancement of Effective Short-Circuit Ratio in a Hybrid Multi-Infeed HVDC System,” *Power Syst. IEEE Trans.*, vol. 28, no. 2, pp. 1568–1581, 2013.

[5] H. Huang and P. a Mawby, “A Lifetime Estimation Technique for Voltage Source Inverters,” *IEEE Trans. Power Electron.*, vol. 28, no. 8, pp. 4113–4119, 2013.

[6] P. Cova and F. Fantini, “On the effect of power cycling stress on IGBT modules,” *Microelectron. Reliab.*, vol. 38, no. 6–8, pp. 1347–1352, 1998.

[7] L. Zhou, J. Wu, P. Sun, and X. Du, “Junction temperature management of IGBT module in power electronic converters,” *Microelectron. Reliab.*, Jul. 2014.

[8] V. Blasko, R. Lukaszewski, and R. Sladky, “On line thermal model and thermal management strategy of a three phase voltage source inverter,” *Industry Applications Conference, 1999. Thirty-Fourth IAS Annual Meeting. Conference Record of the 1999 IEEE*, vol. 2. pp. 1423–1431 vol.2, 1999.

[9] D. A. Murdock, J. E. R. Torres, J. J. Connors, and R. D. Lorenz, “Active thermal control of power electronic modules,” *Industry Applications, IEEE Transactions on*, vol. 42, no. 2. pp. 552–558, 2006.

[10] J. Qin, S. Member, M. Saeedifard, and S. Member, “Reduced Switching-Frequency Voltage-Balancing Strategies for Modular Multilevel HVDC Converters,” vol. 28, no. 4, pp. 2403–2410, 2013.

[11] S. Rohner, S. Bernet, M. Hiller, and R. Sommer, “Modulation, Losses, and Semiconductor Requirements of Modular Multilevel Converters,” *Ind. Electron. IEEE Trans.*, vol. 57, no. 8, pp. 2633–2642, 2010.

[12] ABB, “IGBT Module 5SNA 0650J450300 Data Sheet,” 2012.

[13] Plexim, “PLECS Blockset.” Available in： http://www.plexim.com/.